The insensitive cation effect on single atom Ni catalyst allows selective electrochemical conversion of captured CO_2 in universal media

Jae Hyung Kim,[‡ab] Hyunsung Jang,[‡a] Gwangsu Bak,[‡a] Woong Choi,[c] Hyewon Yun,[a] Eunchong Lee, [a] Dongjin Kim,[c,d] Jiwon Kim, [c,e] Si Young Lee,[a] and Yun Jeong Hwang*[af]

[a]Department of Chemistry, College of Natural Sciences, Seoul National University (SNU), Seoul 08826, Republic of Korea.

[b]Clean Fuel Research Laboratory, Korea Institute of Energy Research, 152 Gajeong-ro, Yuseong-gu, Daejeon 34129, Republic of Korea.

[c]Clean Energy Research Center, Korea Institute of Science and Technology (KIST), Seoul 02792, Republic of Korea.

[d] Department of Material Science and Engineering, Korea University, Seoul 02841, Republic of Korea

[e]Department of Chemical and Biomolecular Engineering, and Yonsei-KIST Convergence Research Institute, Yonsei University, Seoul 03722, Republic of Korea.

[f]Center for Nanoparticle Research, Institute for Basic Science (IBS), Seoul 08826, Republic of Korea.

*e-mail: yjhwang1@snu.ac.kr

Table S1 | Comparison of the cCO_2RR performance of Ni–N/C with those of previously reported catalysts.

Catalyst	Capturing media	Additive	CO_2 flow	Product	Max F. E. (%)	Max j (mA cm^{-2})	Ref.
Ni–N/C	*5 M MEA*	*X*	*X*	*CO*	*65*	*−50*	*This work*
	5 M MEA	*X*	*X*	*CO*	*78*	*-2.6*	
	1 M $KHCO_3$	*X*	*X*	*CO*	*91*	*−4.0*	
Ag	2 M MEA	X	X	CO	5	−0.1	26
Ag	5 M MEA	2 M KCl	X	CO	72	−50	
Pb	2 M 2-amino-2-methyl-1-propanol	0.7 M tetraethylammonium chloride + propylene carbonate	X	$HCOO^-$	50	−25	27
Au	2 M 2-amino-2-methyl-1-propanol	0.7 M tetraethylammonium chloride + propylene carbonate	X	CO	45	−10	
Ag	5 M MEA	X	O	CO	39	N/A	24
	5 M MEA	0.1 wt% CTAB	O	CO	38	N/A	
Bi	5 M MEA	X	O	$HCOO^-$	18	N/A	
Pb	5 M MEA	0.1 wt% CTAB	O	$HCOO^-$	61	N/A	
Cu	Ethylenediamine	X	O	CO	58	−18.4	25
Hg	1 M $NaHCO_3$	X	X	$HCOO^-$	N/A	j_{HCOO^-}: −1	15
Pd	2.8 M $KHCO_3$	X	X	$HCOO^-$	88	j_{HCOO^-}: −3.5	16
Ag	3 M $KHCO_3$	X	X	CO	81	−25	17
Ag	2 M KOH	X	X	CO	28	−100	18
Ag	3 M $KHCO_3$	X	X	CO	80	−20	19
Bi	3 M $KHCO_3$	X	X	$HCOO^-$	82	−100	20
Ag	3 M $CsHCO_3$	X	X	CO	80	−100	21
Ag	3 M $KHCO_3$	X	X	CO	59	−100	22

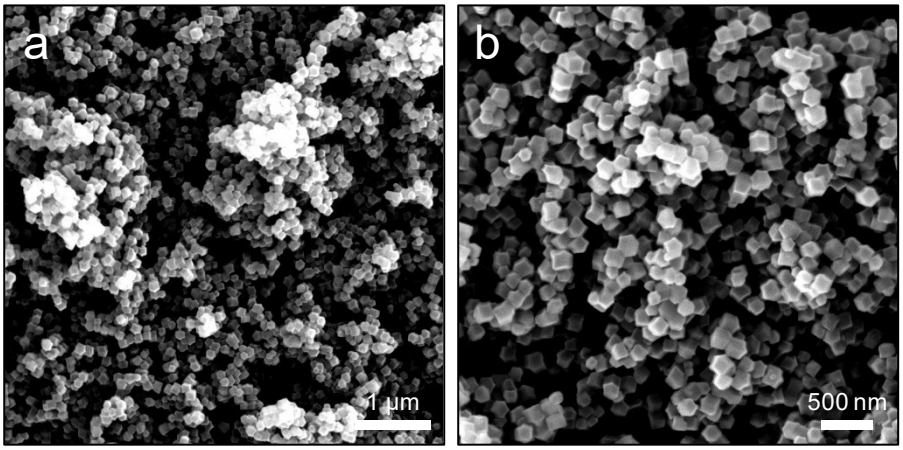

Fig. S1 | a,**b,** Low- (**a**) and high-magnification (**b**) SEM images of ZIF-8.

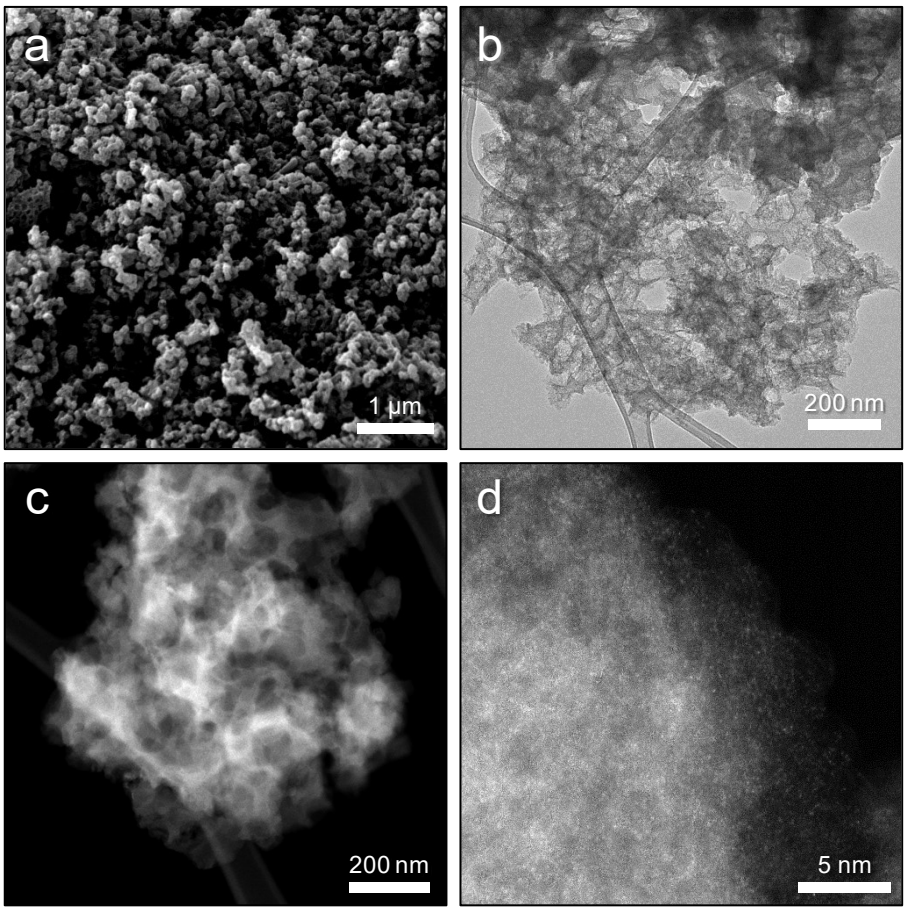

Fig. S2 | a–d, SEM (**a**), TEM (**b**) and HAADF-STEM images (**c**,**d**) of Ni–N/C.

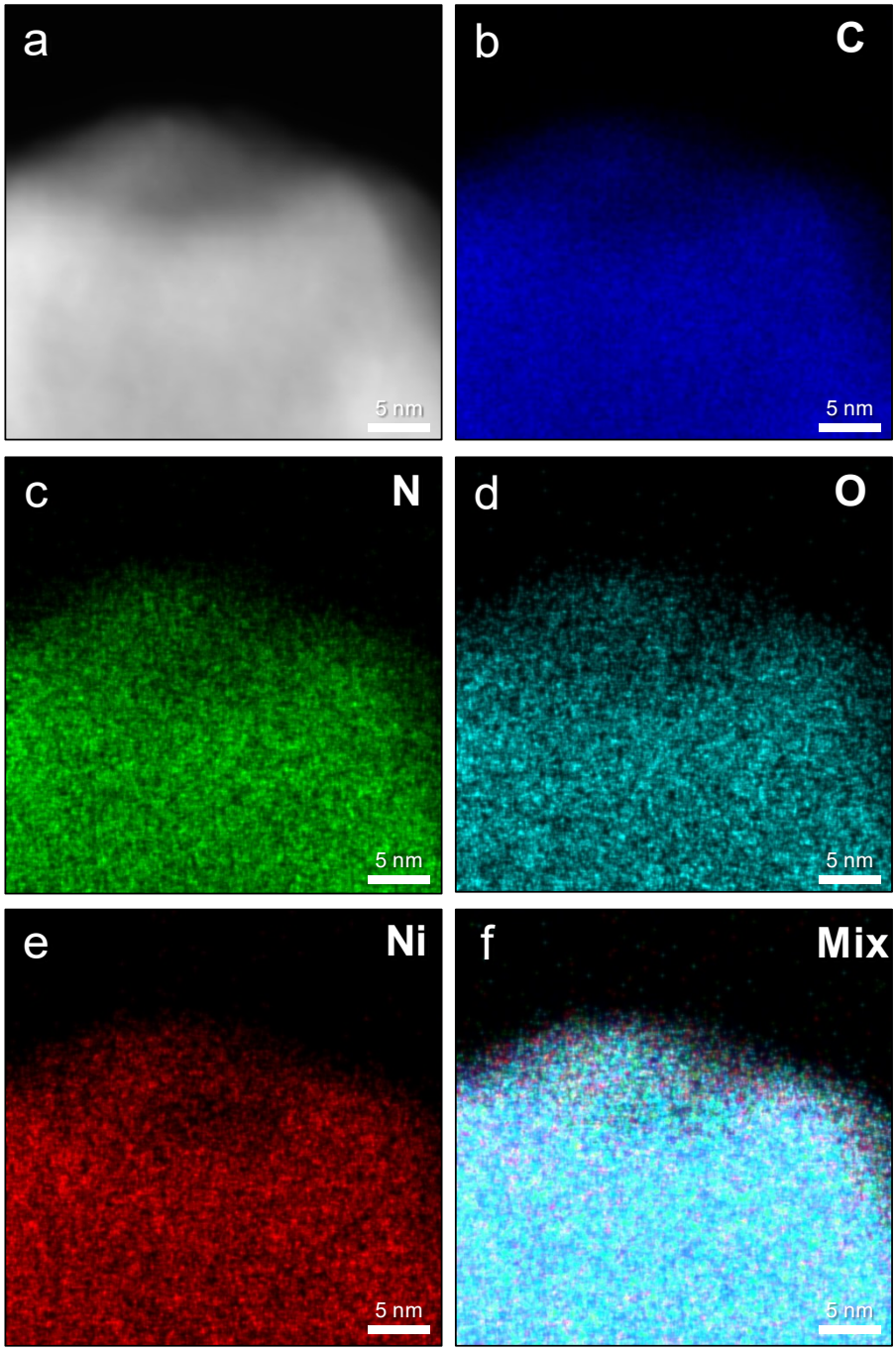

Fig. S3 | a, HAADF-STEM image of Ni–N/C. **b–f**, EDS elemental mapping images of Ni–N/C: carbon (**b**), nitrogen (**c**), oxygen (**d**), nickel (**e**), mixed image (**f**).

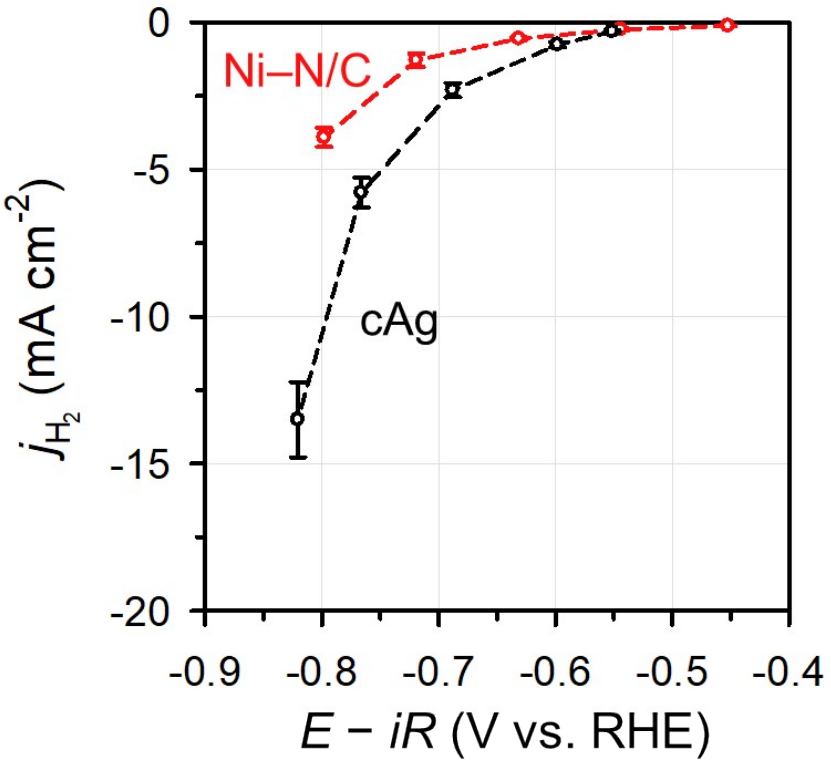

Fig. S4 | H_2 partial current density (j_{H2}) of Ni–N/C and cAg.

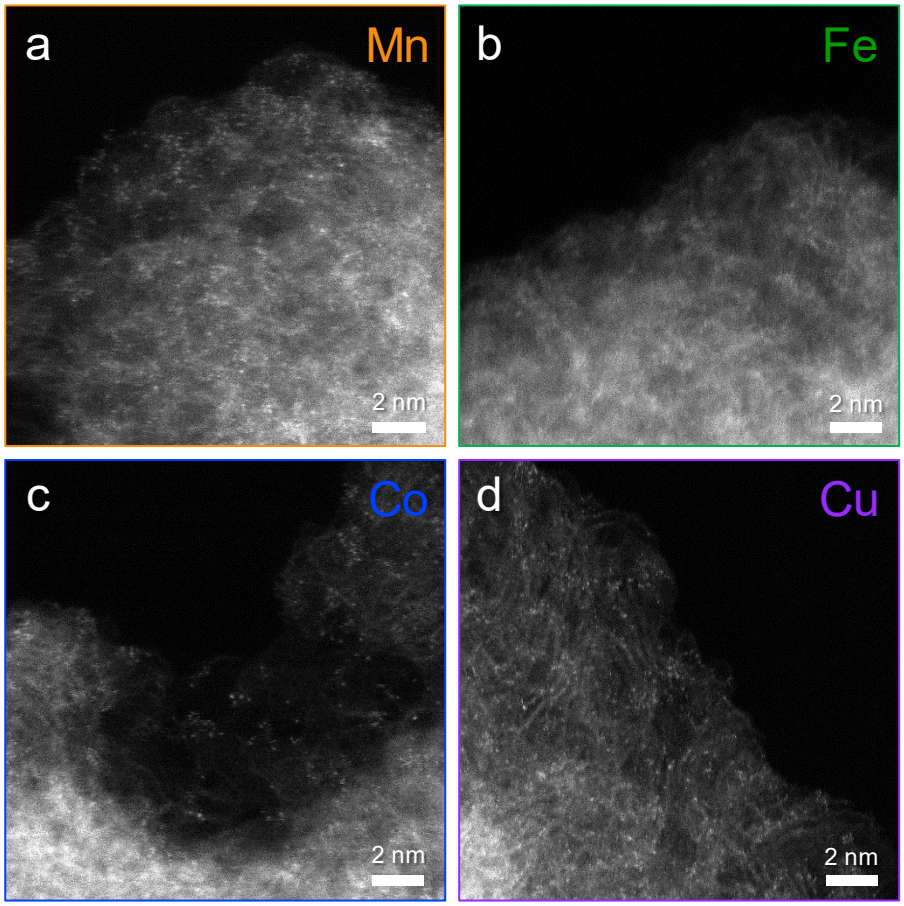

Fig. S5 | a–d, HAADF-STEM images of Mn- (**a**), Fe- (**b**), Co- (**c**) and Cu-based (**d**) single atom catalysts.

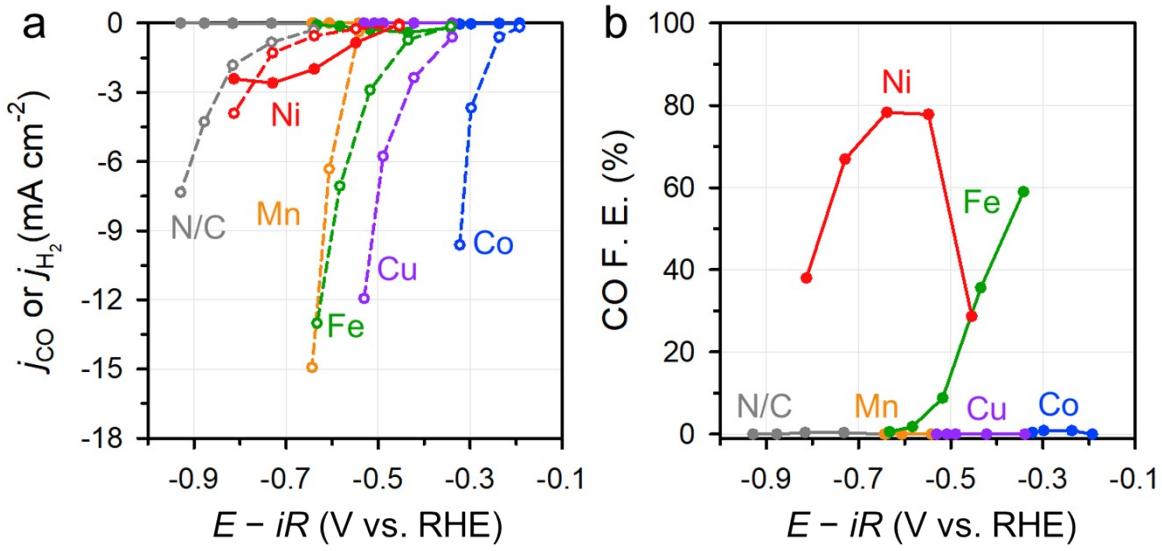

Fig. S6 | a,**b** j_{CO} or j_{H2} (**a**) and CO F.E. (**b**) of various types of single atom catalysts. Solid and dashed lines indicate j_{CO} and j_{H2}, respectively, in **a**.

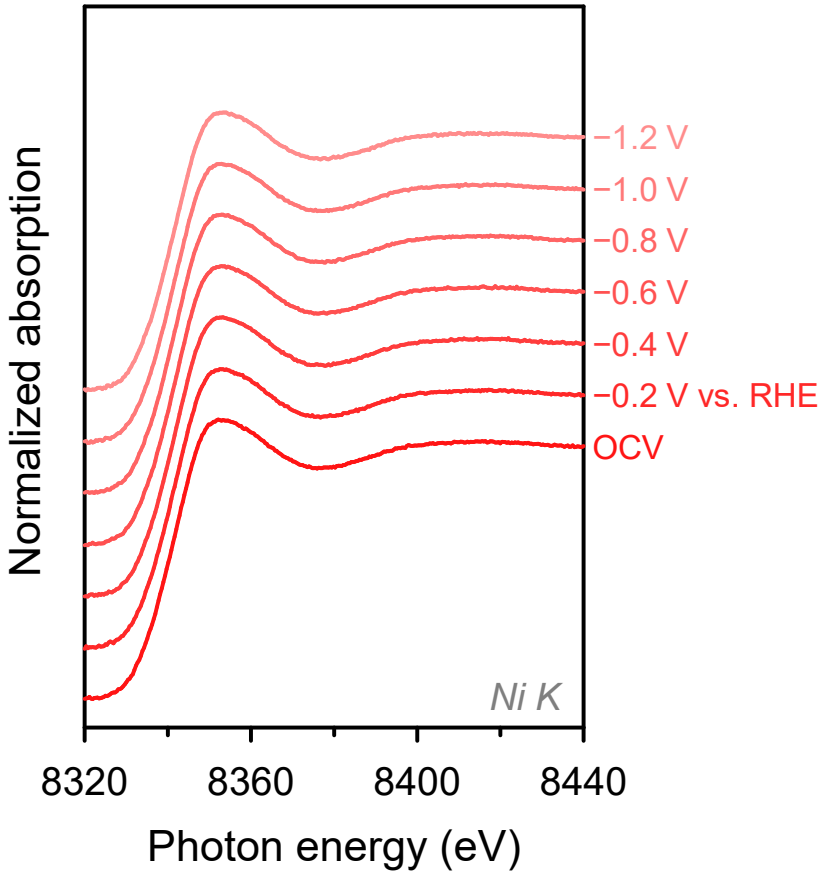

Fig. S7 | Ni K-edge in situ XANES spectra of Ni–N/C taken with applying potential from −0.2 V to −1.2 V vs. reversible hydrogen electrode (RHE).

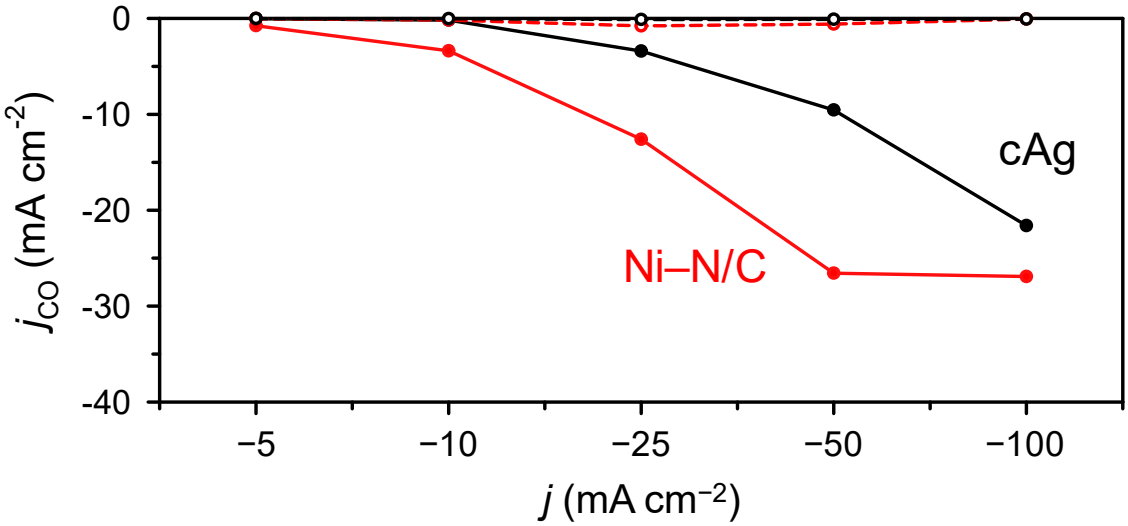

Fig. S8 | j_{CO} of Ni–N/C and cAg at applied constant current density in the membrane electrode assembly test. The solid and dashed lines indicate jco when BPM and AME was used, respectively.

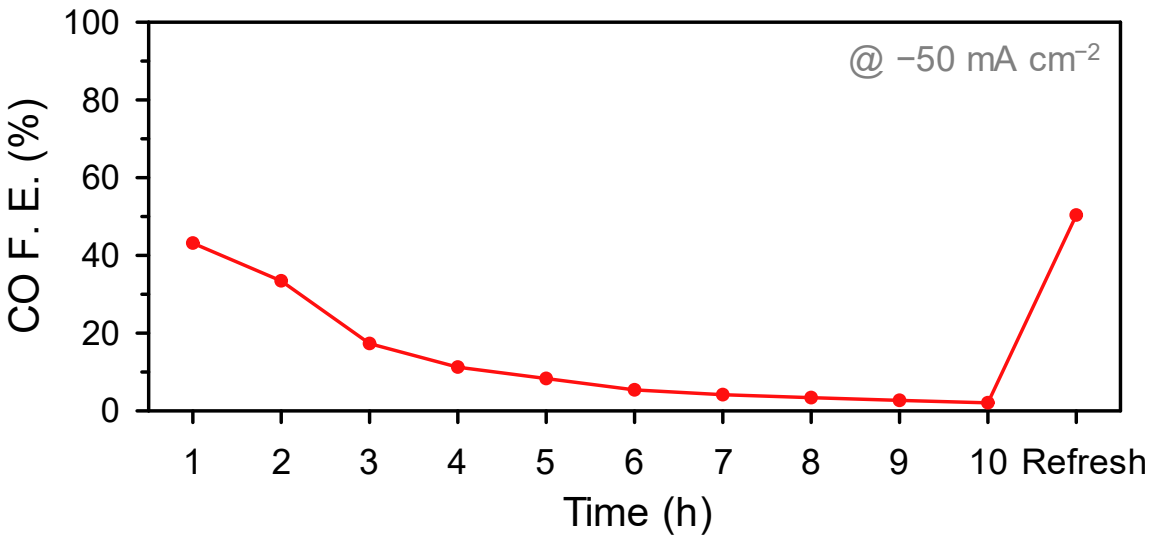

Fig. S9 | CO F. E. changes of Ni–N/C at −50 mA cm^{-2} for 10 h.

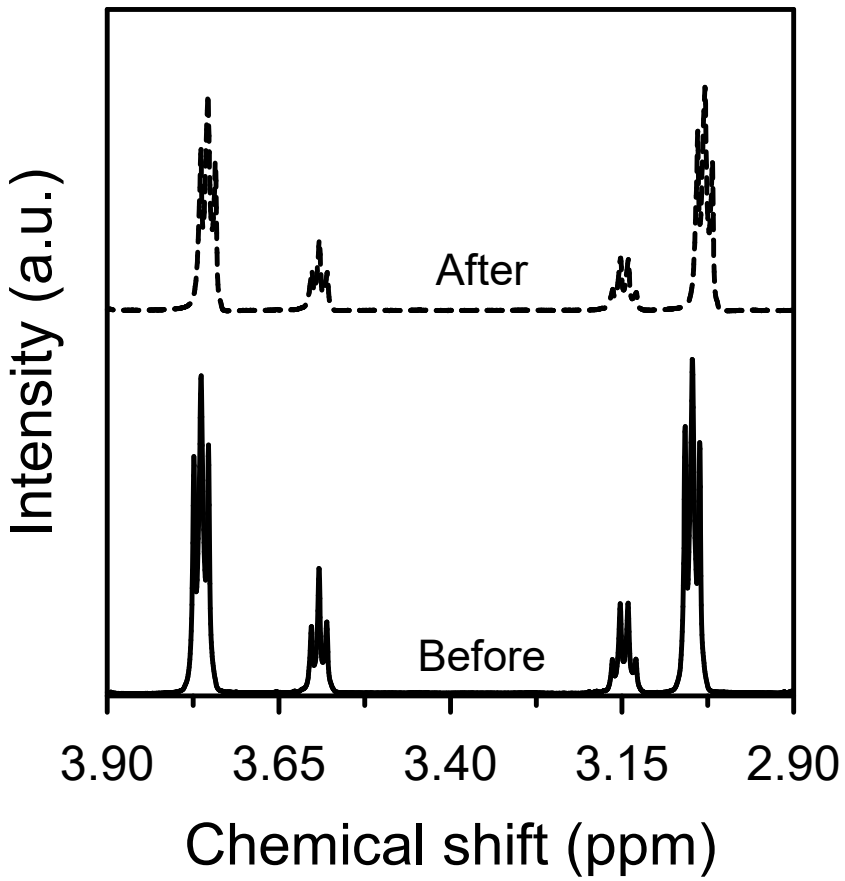

Fig. S10 | ^{1}H NMR spectra of 5 M MEA before and after the electrochemical stability test.

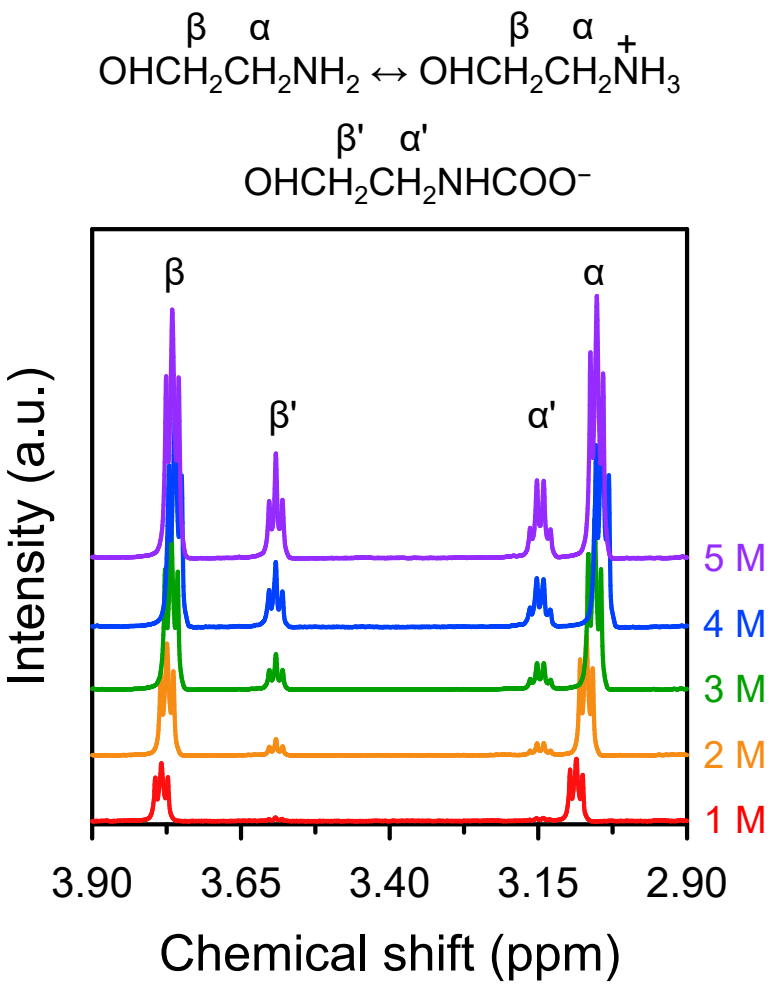

Fig. S11 | ^{1}H NMR spectra of CO_2-adsorbed MEA (1–5 M) solutions.

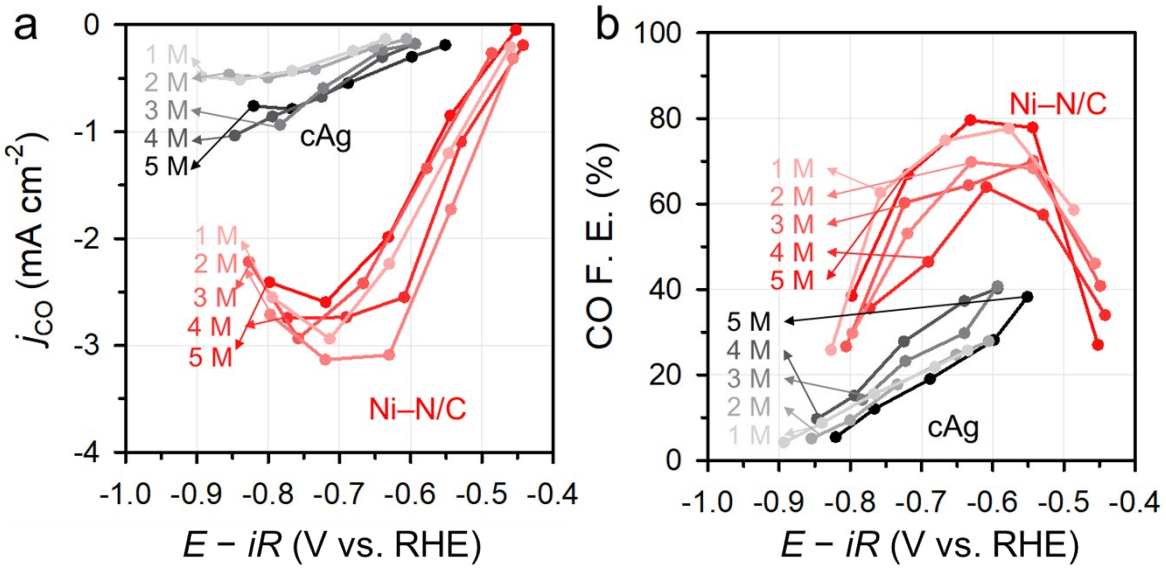

Fig. S12 | a,**b** j_{CO} (**a**) and CO F.E. (**b**) of Ni–N/C and cAg for the cCO_2RR in CO_2-adsorbed MEA (1–5 M) solutions.

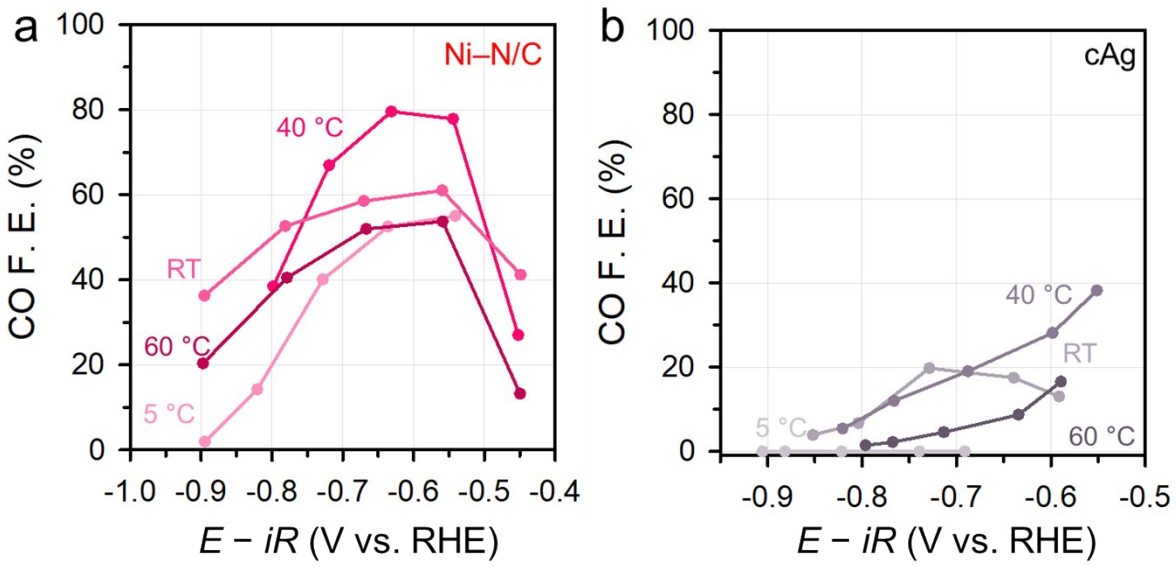

Fig. S13 | a,**b** CO F. E. of Ni–N/C (**a**) and cAg (**b**) for the cCO_2RR in CO_2-adsorbed 5 M MEA in different temperatures.

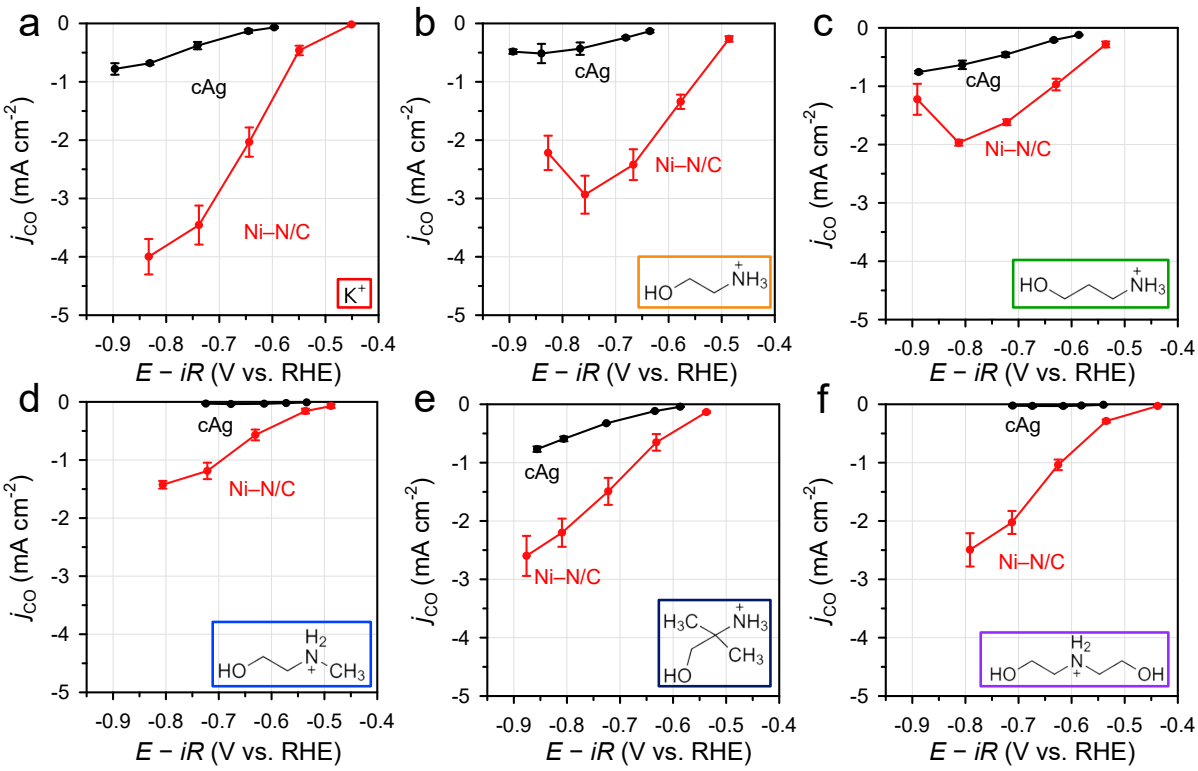

Fig. S14 | a–f, j_{CO} of Ni–N/C and cAg for the direct electrochemical conversion of captured CO_2 in CO_2-adsorbed 1 M $KHCO_3$ (**a**), 1 M MEA (**b**), 1 M 3-amino-1-propanol (**c**), 1 M 2-(methylamino)ethanol (**d**), 1 M 2-amino-2-methyl-1-propanol (**e**) and 1 M diethanolamine (**f**) solutions.

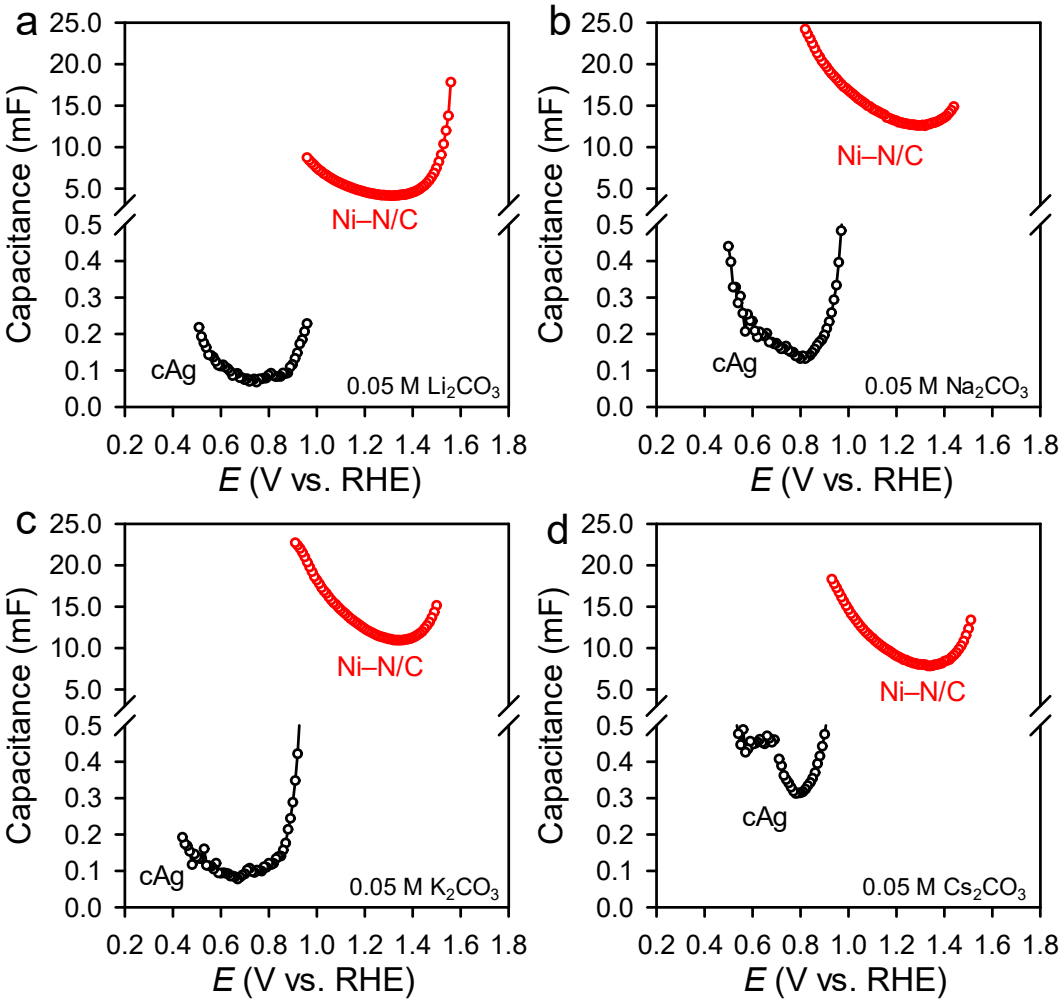

Fig. S15 | a–d, Differential capacity of Ni–N/C and cAg in 0.05 M Li_2CO_3 (**a**), Na_2CO_3 (**b**), K_2CO_3 (**c**) and Cs_2CO_3 (**d**) solutions.

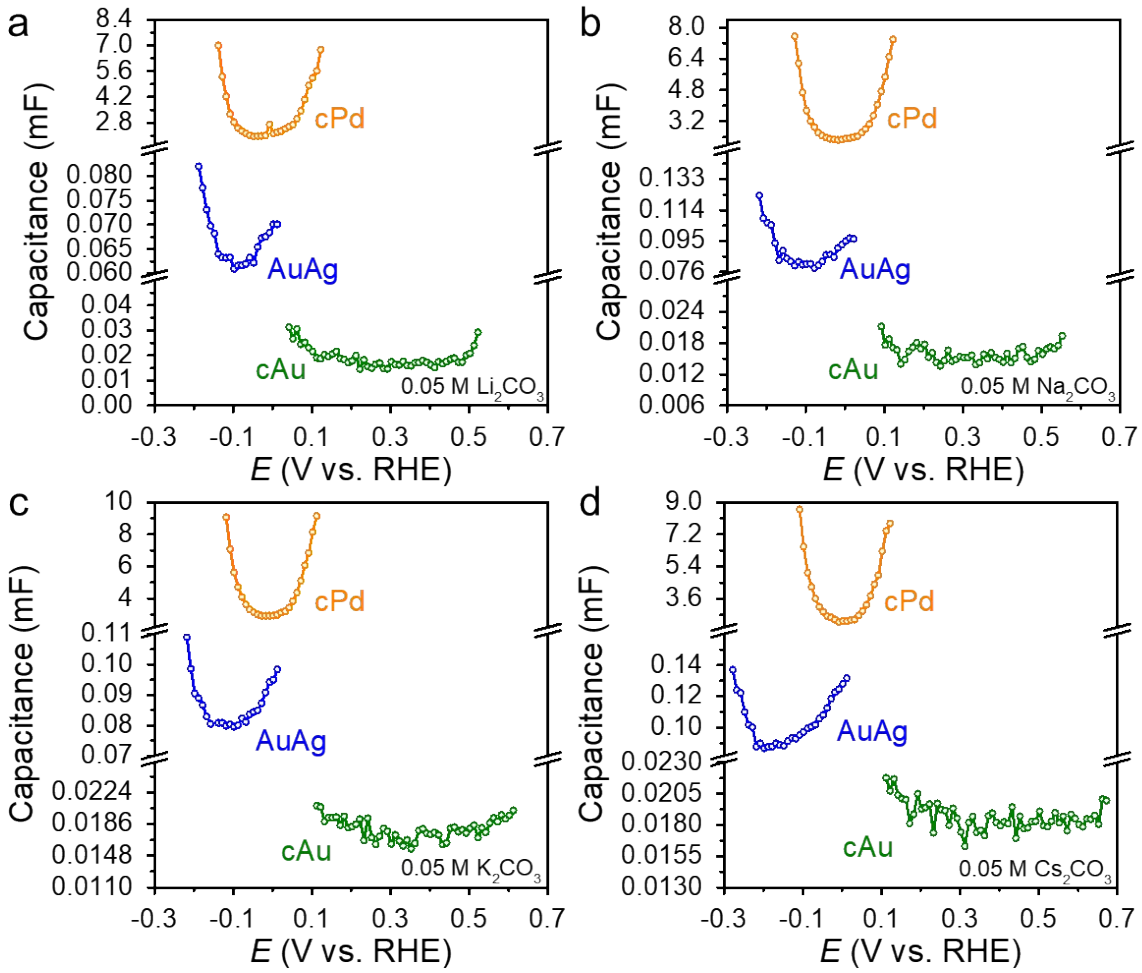

Fig. S16 | a–d, Differential capacity of AuAg, cPd, and cAu in 0.05 M Li_2CO_3 (**a**), Na_2CO_3 (**b**), K_2CO_3 (**c**) and Cs_2CO_3 (**d**) solutions.

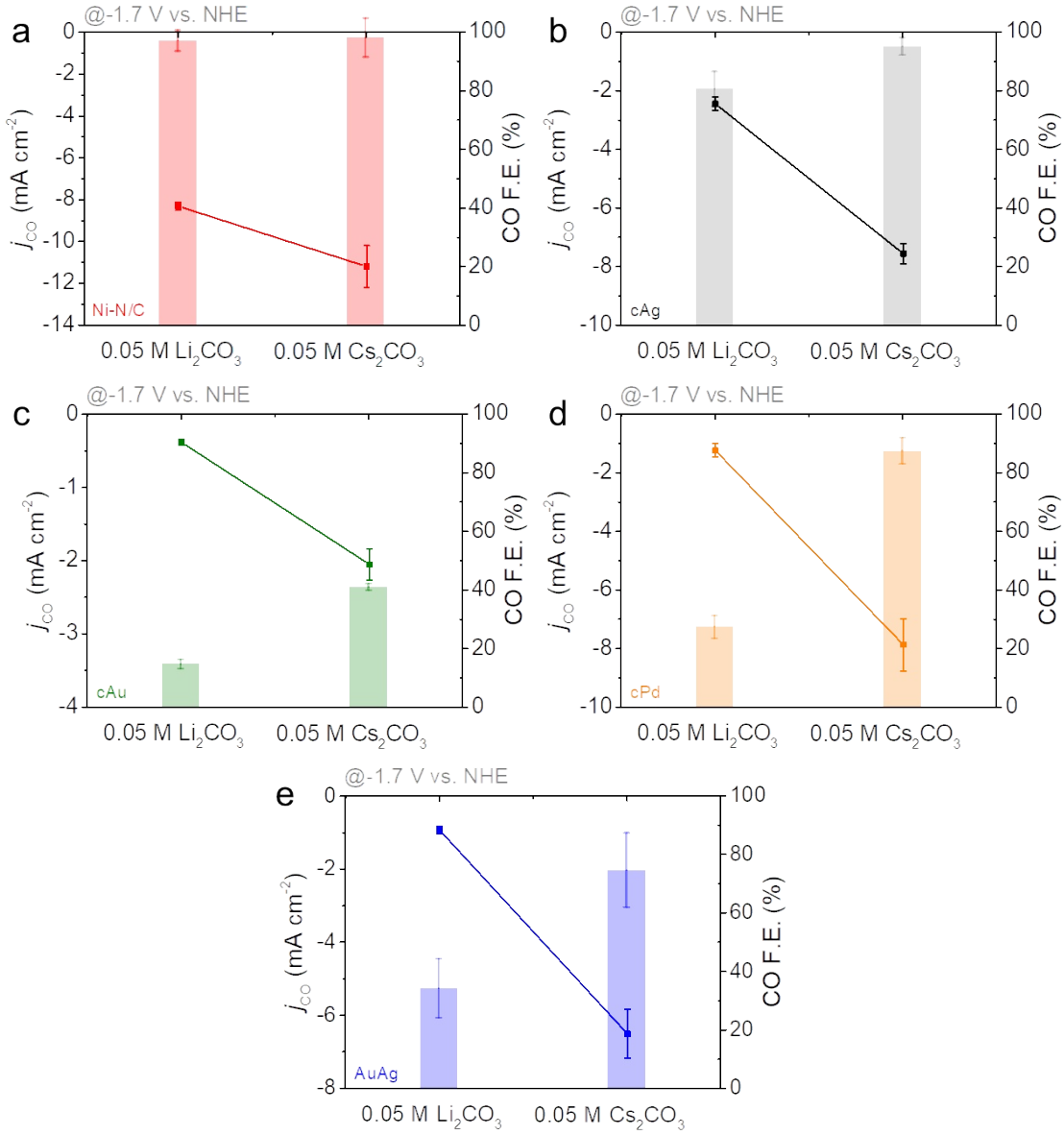

Fig. S17 | a–e, j_{CO} and CO F. E. of Ni–N/C (**a**), cAg (**b**), cAu (**c**), cPd (**d**), and AuAg (**e**) in 0.05 M Li_2CO_3 and Cs_2CO_3 solutions. The scattering plot and bar graph indicate j_{CO} and CO F. E., respectively.

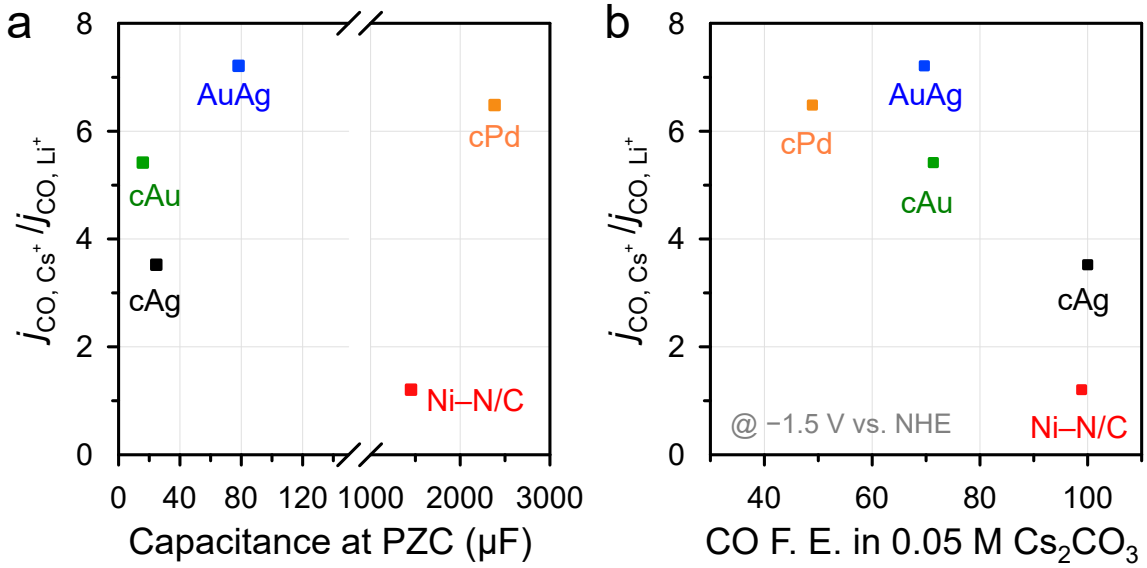

Fig. S18 | a,**b** Relationship between cation sensitivity and capacitance of electrode (**a**) and cation sensitivity and CO F. E. (**b**).

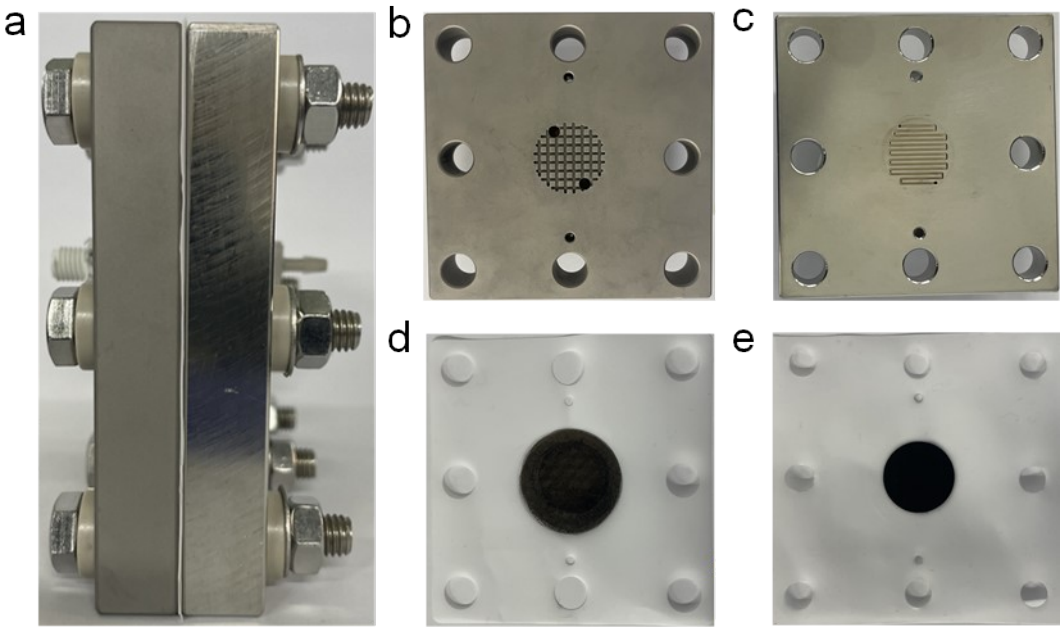

Fig. S19 | a–e, Photographs of assembled custom-designed membrane electrode assembly electrolyzer cell (**a**), flow plates of anode (**b**) and cathode (**c**), gaskets and electrode of anode (**d**) and cathode (**e**).